Thermal Non-Line-of-Sight Imaging from Specular and Diffuse Reflections

Masaki Kaga[1,a)] Takahiro Kushida[1,b)] Tsuyoshi Takatani[1,c)]
Kenichiro Tanaka[1,d)] Takuya Funatomi[1,e)] Yasuhiro Mukaigawa[1,f)]

Abstract

A non-line-of-sight technique is presented to estimate the position and temperature of an object occluded from a camera via reflection on a wall. Because thermal objects emit far-infrared light according to their temperature, their positions and temperatures can be estimated from reflections on a wall. A key idea is that light paths from a hidden object to the camera depend on the the position of the hidden object. The position of the object is recovered from the angular distribution of specular and diffuse reflection components while the temperature of the heat source is recovered from the estimated position and the intensity of reflection. The effectiveness of our method is evaluated in real-world experiments. It is seen that the position and temperature of hidden object can be recovered from the distribution of reflection on the wall using a convectional thermal camera.

1. Introduction

Measuring objects that are hidden from the view of a camera is an important problem in many research fields, such as the fields of robotic vision, autonomous driving, medical imaging, and remote sensing. Non-line-of-sight (NLOS) imaging deals with the problem by reconstructing the position, shape and reflectance of the hidden objects from indirect light paths. Light emitted from a light source reflects from objects multiple times in both line-of-sight (LOS) and NLOS scenes and is then detected by the camera. Although the indirect light paths including reflection from the hidden objects may provide information with which to recover images of the NLOS scene, such an inverse problem is a challenging task.

Most NLOS imaging techniques require a controllable light source to tackle the above task. Meanwhile, we propose a passive NLOS imaging technique that uses far-infrared (FIR) light. Because all thermal objects radiate FIR light in accordance with their temperature, any object in the real world can be regarded a light source at FIR wavelengths. We realized this makes the inverse problem simpler. That is to say, we can formulate the problem as the one-bounce problem, in which a light ray is assumed to be reflected only once, while active techniques assume a three-bounce problem. In our formulation, the light emitted from a hidden object is reflected off a wall in the LOS scene, and then observed by the camera. We assume that the reflection on the wall can be separated into diffuse and specular components, whose light paths depend on the position of the hidden object and whose intensities relate to the temperature. Thus, separating the two components allows us to reconstruct the position and temperature of the hidden object, as shown in Fig. 1. Experimental results show the effectiveness of the proposed method using a conventional thermal camera.

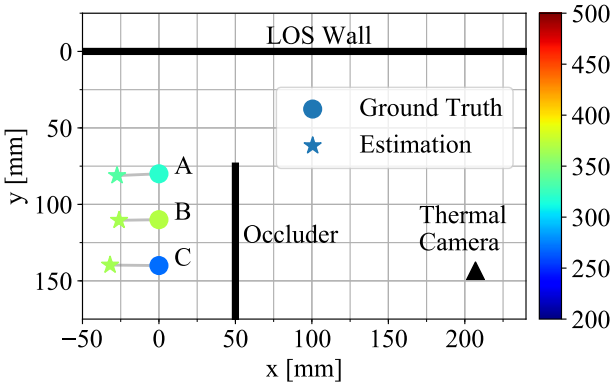

Fig. 1: Experimental results of the position and temperature estimation. Although the target objects are located beyond the occluder, the estimated positions are close to the ground truth. Moreover, the estimated temperatures, shown by color, are consistent with the actual temperatures.

2. Related work

Active NLOS imaging: Most NLOS imaging techniques rely on time-resolved imaging using a controllable light source. Early work used a femtosecond-laser to illuminate a scene and a picosecond-resolution streak camera to obtain time-resolved images [4]. Homodyne time-of-flight sensors are also available to obtain time-resolved images [5] and are thus to be applied in NLOS imaging [3]. Single-photon avalanche diode detectors with time-

[1] Nara Institute of Science and Technology
[a)] kaga.masaki.kj4@is.naist.jp
[b)] kushida.takahiro.kh3@is.naist.jp
[c)] takatani.tsuyoshi.to2@is.naist.jp
[d)] ktanaka@is.naist.jp
[e)] funatomi@is.naist.jp
[f)] mukaigawa@is.naist.jp

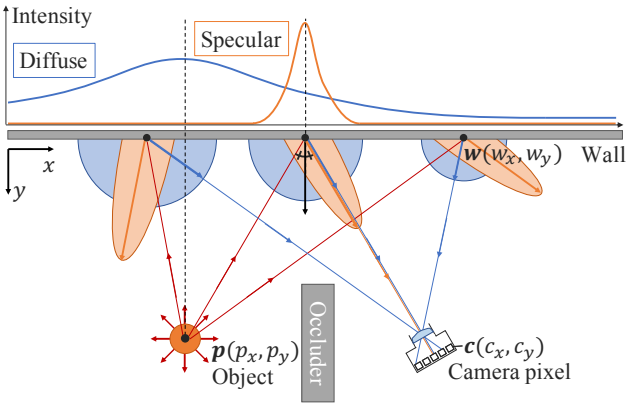

Fig. 2: Geometry setup and concept.

correlated single-photon counting have increasingly been used since they became available and are often used for NLOS imaging [6], [9].

Passive NLOS imaging: A few passive NLOS imaging techniques have recently been proposed. Torralba and Freeman [8] showed that an accidental camera can image a NLOS scene. Bouman *et al.* [2] showed that obstructions with edges, (*e.g.*, walls) can be exploited as a camera that reveals the NLOS scene beyond them. Saunders *et al.* [7] proposed a passive NLOS imaging that requires only a single image captured with an ordinary camera to recover a partially hidden scene and the position of an opaque object in the NLOS scene. Beckus *et al.* [1] proposed a passive NLOS imaging through multi-modal fusion of the intensity and spatial coherence function.

All the existing NLOS imaging techniques expect scenes to be illuminated with light from the visible to NIR. Meanwhile, we use FIR light for passive NLOS imaging that recovers not only the position but also the temperature of the hidden object.

3. Thermal NLOS imaging

We assume that a target thermal object is located beyond an occluder outside the view of a thermal camera. The camera observes a flat wall in a LOS scene on which the FIR light emitted from the hidden object is reflected. We assume that the reflection of FIR light, as well as visible light, can be separated into diffuse and specular reflections and that the geometry and that the geometry of the wall and the camera is given. Figure 2 shows the geometry of the scene. We assume that the hidden object has zero size to simplify the problem.

The present study estimates the position and temperature of the hidden object from a single thermal image. The main idea is that peaks in the intensity distribution on the wall depend on the position of the object. An observed intensity on the image plane can be projected onto the wall because of the known geometry. Considering specular and diffuse components separately, a peak in the intensity distribution for the specular component is around the position where the incident angle is equal to the outgoing angle, as shown in Fig. 2. Meanwhile, a peak in the distribution for the diffuse component is around the position where the distance between the object and wall is minimal. Therefore, once the two distributions are separated, we can estimate the position of the hidden object via the backprojection of expected light paths.

3.1 Separation of diffuse and specular reflections

The observed intensity in the image comprises not only diffuse and specular components but also an ambient component. However, the ambient component can easily be removed by subtracting an observation without the hidden object. The two reflections are separated in the one-dimensional distribution of intensities on the wall. Because a camera pixel $\boldsymbol{c}$ and a point on the wall $\boldsymbol{w}$ have a one-to-one correspondence, we can transform the observed intensity into the intensity on the wall via geometric and radiometric corrections. The intensity on the wall is expressed as

$$I_{\mathrm{w}}(w_x) = D_{\mathrm{w}}(w_x) + S_{\mathrm{w}}(w_x), \tag{1}$$

where D_{w} and S_{w} are respectively the diffuse and specular components.

We now build an empirical model of the diffuse and specular components. Our measurements reveal that the two components follow Gaussian distributions. We define the two components as

$$D_{\mathrm{w}}(w_x) = a_d \exp\left(-\frac{(w_x - \mu_d)^2}{2\sigma_d^2}\right), \tag{2}$$

$$S_{\mathrm{w}}(w_x) = a_s \exp\left(-\frac{(w_x - \mu_s)^2}{2\sigma_s^2}\right), \tag{3}$$

where a_d, μ_d and σ_d^2 are respectively the scale, mean, and variance of the diffuse component and a_s, μ_s and σ_s^2 are respectively those of the specular component. There is the constraint that $\sigma_d > \sigma_s$ because the spatial spread of diffuse reflection is always larger than that of specular reflection. To separate the two components, we optimize

$$[\mu_d, \mu_s, \sigma_d, \sigma_s, a_d, a_s] = \underset{\mu_d,\mu_s,\sigma_d,\sigma_s,a_d,a_s}{\operatorname{argmin}} \sum_{w_x} \left| I_{\mathrm{w}}(w_x) - \hat{I_{\mathrm{w}}}(w_x | \mu_d, \mu_s, \sigma_d, \sigma_s, a_d, a_s) \right|^2, \tag{4}$$

where $\hat{I_{\mathrm{w}}}(w_x)$ is the reconstructed intensity. Figure 3 shows an example of separation.

3.2 Position estimation

The position of the hidden object is estimated by using the separated diffuse and specular distributions. Because the outgoing angle of specular reflection is equal to the incident angle, a light path from a point on the wall $\boldsymbol{w}$ to the object point is expected as

$$\boldsymbol{l} = \frac{\boldsymbol{w} - \boldsymbol{c}}{\|\boldsymbol{w} - \boldsymbol{c}\|^2} - 2\left(\frac{\boldsymbol{w} - \boldsymbol{c}}{\|\boldsymbol{w} - \boldsymbol{c}\|^2} \cdot \boldsymbol{n}\right)\boldsymbol{n}, \tag{5}$$

where $\boldsymbol{n}$ is the normal direction of the wall. In general, specular reflection on a real-world material has blurry lobes. We

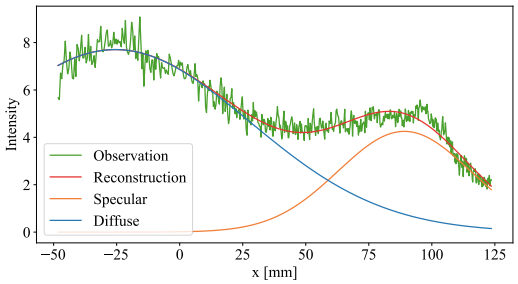

Fig. 3: Separation result. The observed intensity (green) is separated into a diffuse component (blue) and specular component (orange).

thus apply a voting scheme to compute the probability distribution of the position. A light path of specular reflection at each point on the wall is tracked along a direction $\boldsymbol{l}$ in a voting space $\mathcal{V}$ whose y-axis is the normal direction of the wall $\boldsymbol{n}$ and whose origin is on the wall. Although light paths of diffuse reflection are possibly distributed in all directions, the intensity is expected to depend on the distance between the object point and the point on the wall. A light path of diffuse reflection at each point on the wall is thus tracked along the normal direction of the wall. We define a voting value v at a position $(x, y) \in \mathcal{V}$ as

$$v(x, y) = v_d(x) + v_s(x, y), \tag{6}$$

where v_d and v_s are respectively voting intensities derived from two components. The voting intensity for the specular component at the position (x, y) is depends on the corresponding point on the wall and is determined as $w_x = \frac{c_x y + c_y x}{c_y + y}$. The two voting intensities are thus defined as

$$v_d(x, y) = D_{\mathrm{w}}(x), \tag{7}$$

$$v_s(x, y) = S_{\mathrm{w}}\left(\frac{c_x y + c_y x}{c_y + y}\right). \tag{8}$$

Normalizing the voting space results in the probability distribution

$$p(x, y) = \frac{v(x, y)}{\sum_x \sum_y v(x, y)}. \tag{9}$$

Finally, finding the position $(\hat{x}, \hat{y})$ where $p(\hat{x}, \hat{y})$ is a maximum gives us the estimated position of the hidden object.

3.3 Temperature estimation

The temperature of the hidden object is estimated from the separated diffuse distribution and the estimated position. FIR light energy E radiated from a thermal object is directly proportional to the fourth power of the object's thermodynamic temperature T, according to the Stefan–Boltzmann law:

$$E = \sigma T^4, \tag{10}$$

where σ is the Stefan–Boltzmann constant. The radiated light eventually reaches to the LOS wall but is attenuates along the travelling path. The attenuation rate is depends on the distance, as governed by the inverse-square law. The

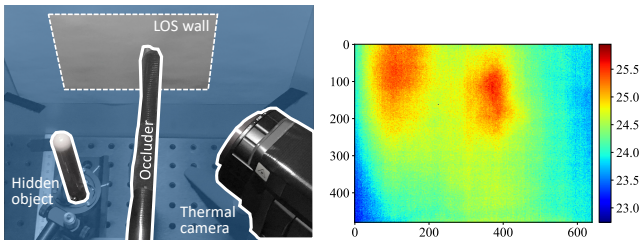

(a) (b)

Fig. 4: Experimental setup: (a) a scene with a hand warmer as the hidden object and (b) an observed thermal image.

light reaching the LOS wall is diffusely reflected from the wall and then recorded by the camera. The scale a_d of the diffuse distribution is thus expressed as

$$a_d = \frac{E k_d}{\hat{y}^2}, \tag{11}$$

where k_d is the diffuse reflectance of the wall and $\hat{y}$ is the estimated distance between the object and the wall. Once the reflectance is obtained (*e.g.*, from the estimated scale under the known distance and temperature), the temperature of the hidden object can be estimated as

$$T = \left(\frac{a_d \hat{y}^2}{k_d \sigma}\right)^{\frac{1}{4}}. \tag{12}$$

4. Experiments

We demonstrate estimations of the position and temperature of a hidden object. In the experimental setup, as shown in Fig. 4(a), a thermal camera (Nippon Avionics, InfRec R500) observes a flat melamine wall in a LOS scene. Printing paper is placed on the wall. A hidden object is located beyond a blackboard in a NLOS scene. Two objects are used as the hidden object: a soldering iron and a hand warmer. The iron can remain at different temperatures of 270, 320, and 370 °C while the hand warmer warms to around 50 °C when plugged in. An observed image is shown in Fig. 4(b) in the case of the hand warmer. An aluminum board with grid holes is used to calibrate the intrinsic parameters of the camera and the geometry between the wall and the camera. The camera and objects are adequately warmed up before starting experiments and the ambient temperature is kept constant during the experiments.

4.1 Position Estimation

First, we evaluate the estimation of position of the hidden object. We locate the iron with a temperature of 370 °C at three different positions A, B, and C in the NLOS scene, as shown in Fig. 1. An observed image is separated into diffuse and specular components for each horizontal line and voting is then performed to get the probability distribution. The probability distribution for each position is shown in Fig. 5(a–c), where the blue circle and red cross respectively denote the ground- truth and the maximum-probability positions. The errors in the estimated positions for A, B, and C are respectively 27.41, 26.07, and 31.94 mm.

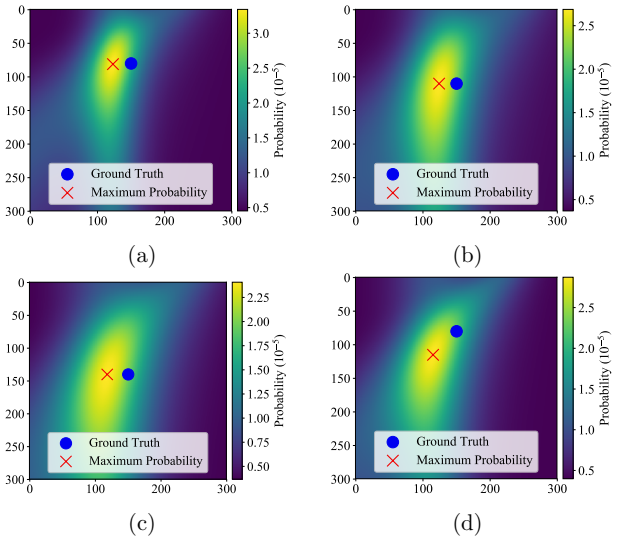

Fig. 5: Experimental results of the position estimation. (a–c) Probability distributions for the position of the soldering iron at the positions A, B, and C. (d) Probability distribution of the hand warmer at the position A. The blue circle and red cross respectively denote the ground-truth and the maximum-probability positions.

Second, the hand warmer, whose temperature is on the order of the temperature of the human body, is located at the position A. The computed probability distribution is shown in Fig. 5(d) and the error in the estimated position is 38.08 mm. The results show that the proposed method can reconstruct the position of a hidden object even at a low temperature.

4.2 Temperature estimation

We demonstrate the temperature estimation of the hidden object. The temperature of the iron is set to 270, 320, and 370 °C for each of the positions A, B, and C. After the positions are estimated, the temperatures are estimated using Eq. (12). The diffuse reflectance k_d is measured ahead by observing the iron with the temperature of 320 °C at the position B. The estimated temperatures are given in Table 1. Because the accuracy of the temperature estimation depends on the position estimation, the error in the position estimation is shown below the estimated temperature. The accuracy cannot to said to be high but the magnitude relationship for each of the positions is at least consistent with that for the actual temperature. The positions and temperatures in selected cases—320 °C at the position A, 370 °C at the position B, and 270 °C at the position C—are shown in Fig. 1.

5. Conclusion

We proposed thermal NLOS imaging to estimate the position and temperature of a hidden object located beyond an occluder. An observed thermal image is separated into diffuse and specular components. Voting values along all possible light paths for both components gives us a probability distribution of position. Once the distance between the object and wall is estimated, the temperature of the hidden object can be inversely be estimated from the diffuse intensity. Experimental results show that the proposed method can estimate the position and temperature of a soldering iron located at different positions and having different temperatures, and the position of a hand warmer, whose temperature is on the order of that of the human body.

Table 1: Experimental results of the temperature estimation. The error in the position estimation. The error in the position estimation is shown below the estimated temperature because the accuracy of the estimated temperature depends on the position estimation.

	270 °C	320 °C	370 °C
Position A	280 °C (27.77 mm)	335 °C (27.41 mm)	351 °C (24.94 mm)
Position B	283 °C (23.79 mm)	N/A (22.98 mm)	365 °C (26.07 mm)
Position C	365 °C (31.94 mm)	441 °C (40.19 mm)	473 °C (36.35 mm)

Limitations: The present paper assumes a single object in a NLOS scene and an adequately simple shape; *e.g.*, a cylindrical shape. Because FIR light radiated from objects is attenuates in the air, the working distance of our method is limited and currently less than 200 mm. When the temperature of a hidden object is low, it is difficult to apply our method because the signal-to-noise ratio of observations is also law. The FIR reflection model is empirically built currently but could be derived from thermal physics and optics, which will be a focus of our future work.

Acknowledgment This work is partly supported by JSPS KAKEN grant JP18H03265, JP17J05602, and JST CREST Grant Number JPMJCR1764.

References

[1] Beckus, A., Tamasan, A. and Atia, G. K.: Multi-Modal Non-line-of-sight Passive Imaging, *IEEE Trans. on Image Processing* (2019).

[2] Bouman, K. L., Ye, V., Yedidia, A. B., Durand, F., Wornell, G. W., Torralba, A. and Freeman, W. T.: Turning Corners into Cameras: Principles and Methods, *IEEE International Conference on Computer Vision*, pp. 2289–2297 (2017).

[3] Kadambi, A., Zhao, H., Shi, B. and Raskar, R.: Occluded Imaging with Time-of-Flight Sensors, *ACM Trans. Graph.*, Vol. 35, No. 2, pp. 15:1–15:12 (2016).

[4] Kirmani, A., Hutchison, T., Davis, J. and Raskar, R.: Looking around the corner using transient imaging, *IEEE International Conference on Computer Vision*, pp. 159–166 (2009).

[5] Kitano, K., Okamoto, T., Tanaka, K., Aoto, T., Kubo, H., Funatomi, T. and Mukaigawa, Y.: Recovering temporal PSF using ToF camera with delayed light emission, *IPSJ Trans. on Computer Vision and Applications*, Vol. 9, No. 1, pp. 1–6 (2017).

[6] O'Toole, M., Lindell, D. B. and Wetzstein, G.: Confocal non-line-of-sight imaging based on the light-cone transform, *Nature*, Vol. 555, No. 338 (2018).

[7] Saunders, C., Murray-Bruce, J. and Goyal, V. K.: Computational periscopy with an ordinary digital camera, *Nature*, Vol. 565, No. 7740, pp. 472–475 (2019).

[8] Torralba, A. and Freeman, W. T.: Accidental Pinhole and Pinspeck Cameras, *ijcv*, Vol. 110, No. 2, pp. 92–112 (2014).

[9] Tsai, C., Kutulakos, K. N., Narasimhan, S. G. and Sankaranarayanan, A. C.: The Geometry of First-Returning Photons for Non-Line-of-Sight Imaging, *IEEE Conference on Computer Vision and Pattern Recognition*, pp. 2336–2344 (2017).